sciendo | Journal of Electrical Bioimpedance | JoEB bioimpedance.net

J Electr Bioimp, vol. 16, pp. 23-34, 2025
Received 9 Feb 2025 / published 12 Mar 2025
https://doi.org/10.2478/joeb-2025-0004

A study on the effect of the number of expansion units in a microfluidic chip on hyaluronidase-free oocyte denudation in mammals

Ashraf Hisham Dessouky [1,2,5], Haitham EL-Hussieny [1], Taymour Mohammed EL-Sherry [3], Victor Parque [4] and Ahmed M. R. Fath El-Bab[1]

1. *Department of Mechatronics and Robotics Engineering, Egypt-Japan University of Science and Technology (E-JUST), Alexandria 21934, Egypt*
2. *Mechanical Engineering Department, Helwan University, Cairo 11792, Egypt*
3. *Department of Theriogenology, Veterinary Hospital, Faculty of Veterinary Medicine Assiut University, Egypt*
4. *Graduate School of Advanced Science and Engineering, Hiroshima University, 1-4-1 Kagamiyama, HigashiHiroshima 739-8527 Japan*
5. *E-mail any correspondence to: ashraf.dessouky@ejust.edu.eg or ashrafhisham41@h-eng.helwan.edu.eg*

Abstract

In Vitro Fertilization (IVF) and Intracytoplasmic Sperm Injection (ICSI) are well-known fertility treatments that, due to resource-intensive, high degree of expertise required, and frequent subpar performances, often yield in high costs for treatment cycles. Microfluidic technology has enabled cost-effective egg-handling procedures towards new assistive reproductive devices: oocytes are subjected to microchannels with jagged surfaces to let shear stress remove undesirable cumulus cells, and microchannels with expansion units facilitate the transport of oocytes in chips. However, although the previous works have studied the influence of shear stress on oocyte denudation and the role of microchannel teeth in optimizing cell handling efficiency, the study of configurations of jagged surfaces and expansion units in microfluidic devices has remained elusive. Also, comprehensive analysis using both computational fluid dynamics (CFD) and real-world microfluidic devices has remained an unexplored area. To fill the above-mentioned gap, this paper studies microfluidics chips with different expansion units to depict the behavior of oocytes when subjected to controlled input flows. The proposed chips were developed and fabricated using a direct engraving CO_2 laser machine on polymethyl methacrylate (PMMA) sheets and bonded in a natural ventilation lab oven, rendering the highly efficient and low-cost microfluidic chips for oocyte denudation. The effect of the expansion units has been investigated in CFD simulation and real lab experimentation with mature buffalo oocytes at a constant flow rate, and a chip with five expansion units arranged in two lines achieved 98.33% denudation efficiency, low-cost fabrication (about 1 USD), and quick fabrication time (about 20 minutes).

Keywords: Microfluidic; oocyte denudation; CO_2 laser; in vitro fertilization; expansion units

Introduction

Research in recent years has associated lower lifestyle scores with infertility [1]. As such, reproductive health can often be linked with anatomical, emotional, and behavioral changes such as increased appetite and fear [2,3]. Disruptions in reproductive processes can significantly impact a woman's fertility and contribute to various reproductive system disorders, whose prevalence has risen in recent years [4,5]. Infertility is characterized as the inability to conceive a child after 12 months or more of uninterrupted, unprotected sexual intercourse [6]. The global prevalence of infertility among couples of reproductive ages varies between 12.6% and 17.5% in specific regions such as the Americas, Western Pacific, Africa, and Europe [7]. And, according to a report from the World Health Organization (WHO), 1 in 6 people are affected by infertility worldwide [8].

Assisted reproductive technology (ART) can be used to treat infertility, e.g., IVF and ICSI [9], and in-vitro oocyte maturation has shown excellent benefits such as reducing the health risks and diminishing ovarian hyperstimulation syndrome (OHSS) [10]. However, despite the widespread availability and the early success in diagnosing and treating infertility, contemporary ART techniques still face several

drawbacks, such as high cost, limited accessibility, and social stigma, becoming unsuitable to patients [11]. The ART procedures have relied on the expertise of skilled individuals and, historically, have lacked the concomitant and required standardization, rendering results that are contingent upon operator skill [12].

To overcome the above-mentioned issues, microfluidics has become a relatively new field involving the study and manipulation of both fluids and micro/nanoparticles in microchannels often manufactured on tiny surfaces [13]. Microfluidics has demonstrated significant advantages in biomedical applications and research [14], especially in ART. Fertilization through microfluidics has been an area of intensive research in pigs and mice when oocytes were subjected to medium flow and semen through small tubes [15–17]. Researchers can also capture restricted-sized functional samples using microfluidic chips, which only need a minimal number of cells [18].

For successful IVF and ICSI, essential processes are essential: sperm sorting, to select the excellent quality, and oocyte denudation, to remove the cumulus cells around the oocyte [19,20]. By forming gap junctions with the oolemma, the cumulus cells often extend the cytoplasmic projections beyond the zona pellucida [21]. In IVF clinics and reproductive procedures, oocytes require denudation from cumulus cells to enable fertilization; this is achieved by immersing the oocyte in the enzymatic action of hyaluronidase and mechanical pipetting to separate cumulus cells from oocytes [22,23]. Hyaluronan comprises repeated disaccharide units of N-acetyl-D-glucosamine and D-glucuronic acid [24]. One of the components of cumulus-oocyte complexes is hyaluronan, which is highly hydrated and viscoelastic [25]. Hyaluronidase treatment causes cumulus cells to disperse from oocytes and the breakdown of the hyaluronan-based matrix surrounding the cumulus cell-oocyte complex (COCs) [26,27]. Human oocytes treated with hyaluronidases had a lower survival rate, fertilization rate, and post-ICSI development rate than untreated oocytes [28–30]. Also, after being treated with hyaluronidase, the fertilization rate of the mouse oocyte dropped. The ability of oocytes to progress to the morula and blastocyst stages was also diminished after being treated with hyaluronidase for 5 minutes or more [31].

The oocyte denudation aims to facilitate the fertilization process by enhancing the injection of sperm into the oocyte [32]. Zeringue et al. manually removed the cumulus cells from individual bovine zygotes (the first stage of the early embryo) [33,34] using a microfluidic system. The proposed device underwent partial removal and reorientation of the cumulus cell mass. Following oocyte denudation, the cumulus-zygote complex passed through a channel being a little wider than the complex itself. Then, the remaining corona cells were extracted from the oocyte using two suction ports smaller than the complex. Denudation of the cumulus-zygote complex requires a manual approach involving switching and regulating fluid flows to position and move one zygote at a time.

Weng et al. [35] have created a microfluidic system to eliminate cumulus cells from mouse oocytes. COCs treated with hyaluronidase traversed a series of irregularly surfaced microchannels. The cumulus cells were removed by the inner wall of the constriction channel during the processing of COCs via a minimum of 100 cycles of expansion and constriction units. The device described by Weng et al. requires intricate manufacturing and use of hyaluronidase, which results in high manufacturing costs and extensive fabrication time due to the use of PDMS. Still, the device inherits all drawbacks from the concomitant use of hyaluronidases. Despite the suitability for microfluidic chips, nontoxicity, biocompatibility, and good thermal stability [36], PDMS still faces drawbacks such as high fabrication costs, time-consuming processing, lower mechanical stability, and the need for specialized bonding techniques, making PMMA a more practical alternative for large-scale and cost-effective applications.

Chen et al. [37] implemented a multi-channel microfluidic chip with a newly designed microcolumn to capture and measure the penetration reaction of three oocytes under varying Cryoprotectant (CPA) concentrations, improving measurement efficiency significantly. Mokhtare et al. [38] created a microfluidic device for contactless oocyte denudation by reshaping surface acoustic waves (SAW). The device uses biocompatible microwells and four interdigitated transducers (IDTs) to create ultrasonic and remove cumulus cells, resulting in total denudation. Zhai et al. [39] developed a robotic system to automate the removal of mouse cumulus cells from oocytes. The system uses vision-based contact detection, oocyte and cumulus cell recognition, automatic calibration, and micropipette aspiration and deposition control, achieving a denudation efficiency of 95.0 ± 0.8%. Fang et al. [40] investigated the recent advances in microfluidic in-vitro fertilization technologies, showing that microfluidics can significantly enhance assisted reproductive technology (ART) by miniaturizing, integrating, and automating various stages of embryo production.

Oocyte denudation in microfluidic chips requires design and manufacturing of channels featuring jagged surfaces and expansion units. Also, realizing the effective and low-cost microfluidic chips are contingent upon materials that are readily and widely available on the market, being biocompatible, transparent, and with no sign of leakage post-bonding. The above-mentioned features are also essential to investigate cell behavior when subjected to distinct configurations of expansion units and jagged surfaces under low-cost and high-quality considerations. Polymethyl Methacrylate (PMMA) is used to manufacture microfluidic chips for several biological applications,

including Deoxyribonucleic acid (DNA) analysis, polymerase chain reaction (PCR), and cell separation [41–43]. Microfluidic chips have been developed using PMMA for sperm sorting and optimization based on the rheotaxis approach [44,45]. Micro biosensors have been fabricated with PMMA material [46]. Furthermore, several researchers have previously investigated the micromachining of PMMA via a CO_2 laser [47–51]. The direct engraving approach produced several microfluidic chip materials using a laser beam in several bio-applications [52–54]. Microfluidics has been used to explore the transport mechanism of Hg(II) [55] and evaluate the critical suitability of Caco-2 cells [56] as gut-on-a-chip.

Despite the advances in microfluidics to investigate cell behavior in fertilization fields, the study of configurations of oocyte behavior when subjected to distinct configurations of expansion units and jagged surfaces under low-cost and high-quality considerations has remained elusive. The comprehensive analysis utilizing both computational fluid dynamics (CFD) machinery and real-world fabricated microfluidic devices has remained an unexplored area in literature. To fill the above-mentioned gaps, this paper studies microfluidics chips with different expansion units to study the behavior of oocytes when subjected to controlled input flows. As such, it becomes possible to identify the suitable configuration to achieve the highest oocyte denudation performance at a low cost and with a quick fabrication time. Our contributions are as follows:

- Conducted CFD simulations to analyze the effect of wall shear stress on oocytes in different microfluidic chip designs with varying expansion unit lengths and flow rates.
- Experimentally validated the simulation results by fabricating the corresponding microfluidic chips using CO_2 laser engraving.
- Performed real-world oocyte denudation experiments using buffalo oocytes to assess the effectiveness of the designed chips.
- Evaluated oocyte denudation performance based on the denudation success rate (efficiency) under different expansion unit configurations.

In the rest of the paper, we introduce the materials and methods and then discuss the results we obtained.

Materials and methods

Selecting the designs

The dimensions of microfluidic chips correspond to the conventional size often used in microscope slide format, measuring 75.5 x 25.5 mm. Microfluidic chips have been fabricated using 3 mm thick and 0.1 mm PMMA sheets. The chips include three PMMA layers: the upper layer is 3 mm thick and serves as the cover with input and output apertures, while the middle layer is 0.1 mm thick and thoroughly engraved with the necessary design, and the bottom layer is 3 mm thick and serves as a cover to close the microfluidic chip; hence, the overall height of the chip is 6.1 mm.

Oocyte denudation requires the removal of the cumulus-oocyte complex matrix from the oocyte. Consequently, microfluidic channels need internal jagged surfaces with precise width and depth dimensions dependent upon the oocyte's size. Typically, mammalian oocytes are round, with a diameter of 80 µm in mice and 120-130 µm in bigger animals like humans [57]. The average diameter of the buffalo oocytes removed from normal ovaries was 146.4 microns [58]. When accompanied by cumulus cells, the oocyte may be as large as 350 to 450 µm in diameter. Thus, the channel depth is constant due to the thickness of the middle layer. The inner jagged width design is 0.1 mm. The overall channel length is 62.76 mm.

The first chip (labeled as **chip A**) consists of two channels with different numbers of expansion units. One channel has one expansion unit, and the other has 19 expansion units, both at the same length of 62.76 mm. The inlet and outlet holes are 2.00 mm in diameter. Figure 1 represents the diagram of the **chip A**.

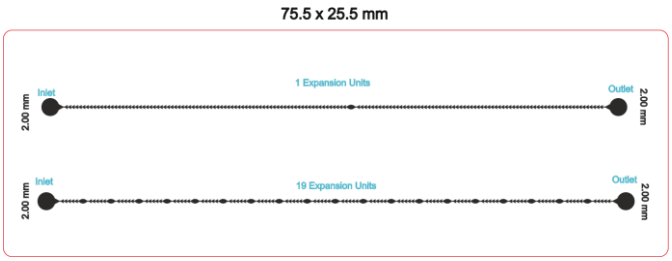

Fig.1: Schematic diagram of chip A.

The jagged surface must have an angle against the flow direction to remove the cumulus cells from the oocytes. The jagged surface mechanically removes the cumulus cells without needing enzymatic action like hyaluronidase. It applies direct shear stress on the oocyte to detach the COCs. The microfluidic chip ensures complete denudation without manual handling and operator variability. According to the literature, the best angle to remove the COCs is almost 141° [35]. Figure 2 (a) shows the teeth angle; the inner width is 0.1 mm, and the distance between each tooth is 0.1 mm.

The expansion units' effect is crucial. They improve fluid dynamics for soft cell processing and facilitate a more effortless transfer of oocytes through the chip. They also optimize the shear force upon the oocyte to remove the COCs and avoid destroying the oocytes. The expansion units will guarantee that all faces of the oocytes are exposed to the jagged surfaces. Figure 2 (b) describes the dimensions of the expansion units. The maximum height (thickness) is 0.5 mm, and the maximum width is 1.00 mm. The chip has a constant depth of 0.1 mm.

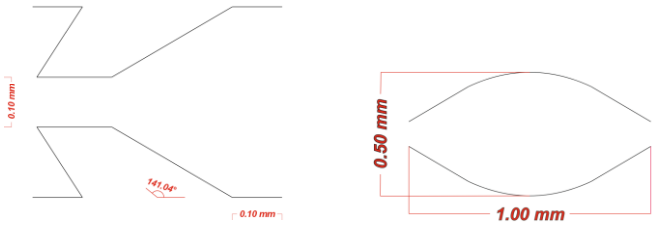

(a) (b)

Fig.2: Detailed schematic diagram of the jagged teeth and expansion unit. (a) Jagged teeth dimensions, (b) The expansion unit dimensions.

The key motivation behind rendering **Chip A** is to allow for a direct comparison of minimal versus extensive expansion unit implementations, ensuring optimized shear stress application. The impact of expansion units will be studied by increasing the number of expansion units and the microfluidic channel length while maintaining the same width and depth. This might be considered a case study.

The second chip (labeled as **chip B**) comprises two lines measuring 64.86 mm, with five expansion units. Figure 3 shows the second microfluidic channel. The connection between the upper and lower channels is considered an expansion unit with a larger space because the thickness of this connection channel is 0.5 mm. The motivation in studying the configuration of **Chip B** is to outline the performance frontiers of a multi-line design, assessing how interconnected expansion units influence oocyte transport and denudation.

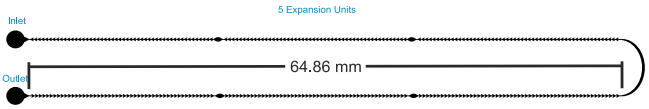

Fig.3: Schematic diagram of chip B.

In line with the above configurations, another study increased the number of expansion units and channel lines, labeled as **chip C**. Figure 4 describes the third microfluidic **chip C** with 99 expansion units and five channel lines. The connection channels are also considered expansion units.

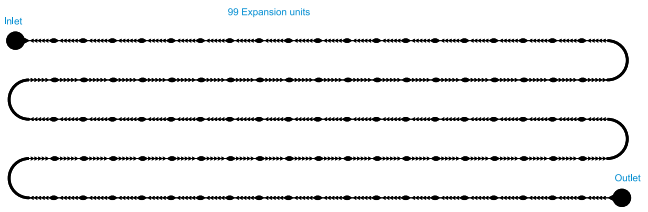

Fig.4: Schematic diagram of the third denudation chip

The key motivation in including **chip C** in our study is to further increase the complexity of the configuration by involving multiple expansion units and channel lines, enabling a comprehensive analysis of fluid dynamics.

The above-mentioned three chips will undergo CFD simulation to evaluate the effect of shear stress and real lab experimentation using actual buffalo oocytes to assess the denudation efficiency, depending on the number of expansion units at the channel length. All chips possess a uniform depth and an interior teeth width of 0.1 mm. The mean angle of all teeth across all chips is 141°.

Fabrication Methodology

The fabrication utilized a CO_2 laser machine (VLS3.5, Universal Laser Systems, Kanagawa, Japan) with a 30-watt laser tube. A laser lens (HPDFO, Universal Laser Systems, Japan) with a 30 µm focal spot was utilized. Microfluidic chips were fabricated using PMMA sheets that were 3 mm thick for the top and bottom layers and 0.1 mm thick for the design layer. To achieve high-quality results, the laser beam for patterning PMMA sheets was adjusted to 1000 pulses per inch (PPI). The laser power was set to 30% and the speed to 40% to achieve the optimal dimensions as specified in the design. The chip is composed of three layers of PMMA. The chip design was executed using CorelDraw x5. The design was thoroughly engraved on the middle layer, whereas the inlet and outlet were drilled into the top layer. The three layers were thermally adjusted and bonded in a natural ventilation laboratory oven (STF-N 80, FALC Instruments, Treviglio, Italy) for 13 minutes at 150 °C under a force of 2 Newton. Subsequently, connection tubes with an outer diameter of 1.8 mm (ULTRAMED, Assiut, Egypt) were attached and secured at the inlet and outlet openings. The tube has an outer diameter of 1.8 mm, while the inlet and outlet holes measure 2 mm. Consequently, a PMMA cylinder with an outer diameter of 2 mm and an inlet diameter of 1.8 mm was incorporated to connect the tubes to the holes, ensuring a leak-free connection. Figure 5 shows the actual fabricated chips.

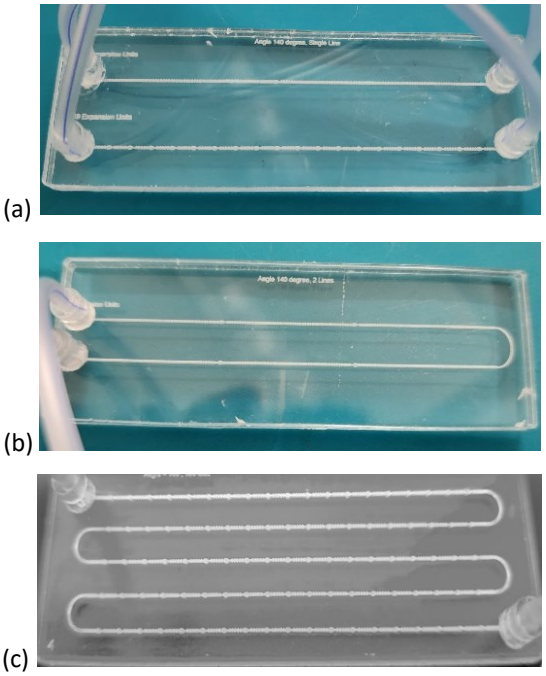

(a) (b) (c)

Fig.5: The Fabricated Chips with the connected tubes. (a) Chip A. (b) Chip B. (c) Chip C.

After the middle layer was fabricated, the channel width was measured using a Fluorescent Trinocular Compound Microscope - AmScope (FMSYG580TA) Supplies 40x–1600x Infinity Plan EPI. The advantage of the three-layer fabrication is that it ensures channel depth. After bonding the chip, further measurements using the same method were performed to confirm the dimensions' stability. Our methods achieved high dimensional stability after fabrication and bonding, almost matching the design. A syringe pump (NE-4000 Pump Systems Inc.) was used to inject deionized (DI) water into the chip from the input to test for leakage. There was absolutely zero leakage consequently. To test and study the thermal effect of the bonding technique, a higher bonding force was applied for 13 minutes at 150 degrees Celsius, which is lower than the melting temperature of PMMA. Chip deformations and some changes in dimensions were noticed. On the other hand, when applying a lower bonding force, air bubbles and leakage were obtained. Therefore, the optimal condition is using the force at 2 Newton at 150 degrees Celsius for 13 minutes in a natural ventilation lab oven to achieve a high transparency chip with no leakage and suitable dimensions compared to the design.

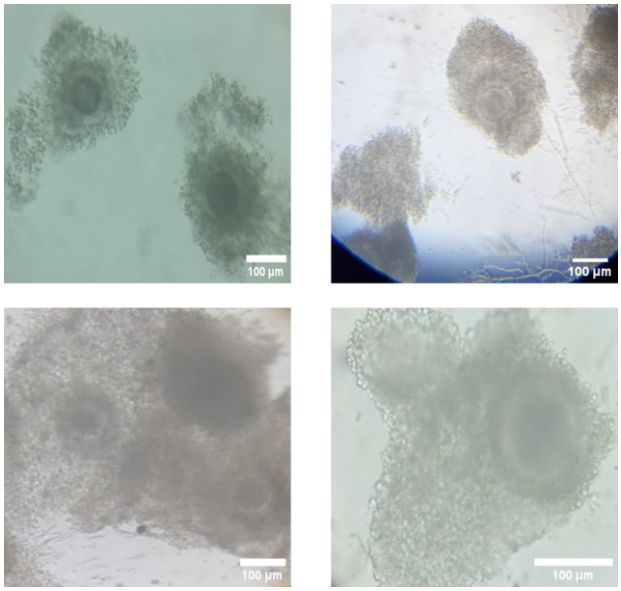

Fig.6: Different shots of the Mature oocytes with cumulus cells under the microscope.

Preparation of the Oocytes

The ovaries of female slaughtered buffalo are obtained from the Dachlout abattoir in Dayrout, Assiut Governorate, which are then transported to the Veterinary Medicine department at Assiut University to undergo washing and cleaning procedures to facilitate the extraction of oocytes. The process is essential as it involves the extraction of oocytes from the ovaries while maintaining integrity. Subsequently, the oocytes are placed in Tissue Culture Medium 199 (TCM 199) (BIO-CHEM, Belgium) and some other materials with specific concentrations for preservation and maturation, as described in Table 1. During the maturation process, oocytes in media were placed in small tubes within a CO_2 incubator (N-BIOTEK Co, Korea) set at 38 degrees Celsius with 5% CO_2 for a duration of 22 to 24 hours, preparing them for the subsequent denudation process. Figure 6 shows the oocytes after maturation (metaphase II) with the cumulus cells around them, which harden fertilization. Although the cumulus cells harden the fertilization, the COCs around the oocytes are vital because they regulate oocyte maturation and meiotic resumption [59]. It also creates metabolic cooperation between the COCs and the oocytes [60] and intercellular communication within the COC is crucial for oocyte development [61].

Table 1: The maturation media concentrations [62].

Component	Final Concentration
TCM 199	9 ml
Fetal Bovine Serum	1 ml
Amphotericin B	1 ml
FSH	10 µl
Sodium Pyruvate	20 µl
Gentamycin	10 µl
Estradiol 17β	10 µl

Mathematical Equations

The primary aspect to consider is the wall shear stress cumulus oocyte cells will encounter when subjected to the jagged units that eliminate all cumulus corona cell mass. The flow rate must be adequate to eliminate cumulus corona cell mass while ensuring the preservation of oocytes, as shear stress is directly proportional to the flow rate. Microfluidics can be modeled mathematically. The most commonly used mathematical models in microfluidics are based on the steady-state Navier–Stokes equation for a Newtonian fluid [63,64].

$$\frac{\partial u}{\partial t} + (u \cdot \nabla)u - \frac{\mu}{\rho}\nabla^2 u = -\frac{1}{\rho}\nabla p + g \qquad (1)$$

where u is the normalized flow velocity vector, p is the pressure, t is the time, ρ is the fluid's density, ∇ is the divergence, μ is the dynamic viscosity, and g is the gravitational constant. In microfluidic systems, surface forces outweigh volume forces like gravity [65]. Therefore, gravitational force may be ignored. Furthermore, the fluid is incompressible, which removes velocity gradients within the fluid volume [66]. With these assumptions, equation (1) can be simplified to the following:

$$\frac{\partial u}{\partial t} - \frac{\mu}{\rho}\nabla^2 u = -\frac{1}{\rho}\nabla p \qquad (2)$$

An analytical solution for velocity profiles in rectangular-based microfluidic channels was found by expanding the Navier-Stokes equation using the Fourier series [67]. However, in simple geometry, such as a wide rectangular or tubular channel, computational fluid dynamics was utilized

to determine the wall shear stress as a function of the channel width and flow rate. Mathematically, the wall shear stress can be calculated in rectangular channels using the following equation [68,69].

$$\tau = \frac{6\eta Q}{h^2 w} \quad (3)$$

where h is the channel height, w is the channel width, Q is the flow rate, and η is the medium viscosity. The viscosity of the TCM 199 medium with other mediums is 0.0011 Pa·s (Pascal Second). The velocity can be calculated using the following equation:

$$Q = A \cdot v \quad (4)$$

where A is the area, and v is the velocity. We inject the fluid constantly, but the velocity will change inside the microfluidic channel. Therefore, the shear stress changed at each point, and consequently, Computational Fluid Dynamics (CFD) is required to calculate the parameters at each point after meshing analysis.

Computational Fluid Dynamics (CFD) Simulation of Velocity and Shear Stress

A three-dimensional (3D) model of each design in the microfluidic chips was conducted on Ansys Fluent 2023 R2 (ANSYS, Inc., Canonsburg, PA) to evaluate and calculate the wall shear stress affected on the oocytes. The geometry was constructed by drawing our design with accurate lengths and widths on the geometry part in the Ansys Fluent project. Then, the design was extruded with a 0.05 mm depth in both-symmetric to get 0.1 mm depth. The design was established as an actual chip design. A named selection was created in the meshing part to specify the inlet, outlet, fluid domain, and wall. The wall is assumed to be the whole design without the inlet and outlet. Then, geometry and material were selected, and an automatic method for meshing was used. The element size was selected and then reduced more and more until the same output results were obtained. After many trials, an element size of 10 µm in the body sizing analysis was found enough to ensure high accuracy without changing the output results if we reduce it. Figure 7 shows the meshing analysis in Ansys, specifying the element size.

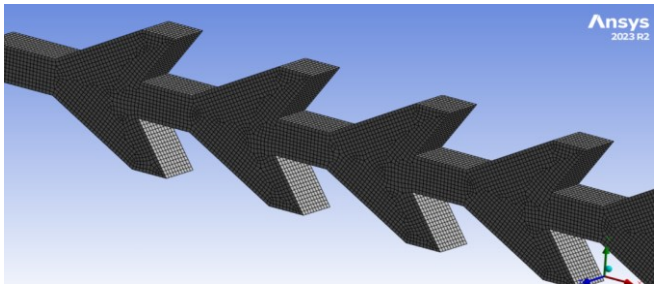

Fig.7: Meshing analysis in Ansys.

Double precision is selected in the setup and solution section, the time is steady, and a laminar flow (due to the Reynold number) is selected with specified fluid parameters such as viscosity. The viscosity of the TCM medium with other mediums is 0.0011 Pa·S (Pascal Second). The flow rate will be changed to see the shear stress effect.

Experimental Denudation Process

After preparing the oocytes, 0.5 mL of media with about 15 oocytes was transferred to an Eppendorf tube. A micro-pipette to manipulate the 0.5 mL volume is essential to avoid oocyte adhesion to the tube's walls or bottom. The pumping technique employed in this context is distinct. If fluid is pumped from the inlet to the outlet, it will remain in the tube and not enter the microfluidic chip. Consequently, an alternative pumping technique was employed. The output tube was connected to a 10 mL sterile syringe (Jiangxi Hongda Medical Equipment Group, Nanchang, China) and placed into a syringe pump (NE-4000, New Era Systems, Grant, FL, USA). In comparison, the input tube was inserted into the micro-Eppendorf tube. Subsequently, the flow rate was adjusted. The withdrawal operation is initiated to extract the fluid from the reaction tube, traverse the designated channel, and collect the fluid in the syringe.

All fluid was rapidly injected through the channel, ensuring no fluid remained in the input tube and the input tube was not removed from the syringe, nor was air infused to facilitate fluid movement to the channel. The injected fluid was subsequently stored in the medium syringe that contained the denudated oocytes. To determine the output results, an MT5000(IFR) 5.0MP CCD fluorescent microscope camera, which has a Sony ICX282AQ sensor, was mounted on the Fluorescent Trinocular Compound Microscope – AmScope (FMSYG580TA). The microscope and the camera are connected to the lab computer to see the results.

Ethical approval

The conducted research is not related to either human or animal use.

Results

Computational Fluid Dynamics (CFD) Results

In the Ansys results section, the wall shear stress was studied. The maximum shear stress occurs at the beginning of the first pair of teeth. Different flow rates were applied to evaluate the effect of varying the number of expansion units upon the shear stress. Figure 8 describes the maximum shear stress applied to each design's first pair of teeth at different flow rates, such as 0.25, 0.5, 0.75, 1, 1.25, and 1.5 mL/min.

Figure 8 illustrates a negligible difference across the designs, indicating that various numbers of expansion units do not influence the shear stress exerted on the oocytes. These chips will undergo testing with actual oocytes in the laboratory to evaluate denudation efficiency. Figure 9 (a), (b), (c), and (d) present the CFD simulation results (vector or contour) for the three chips.

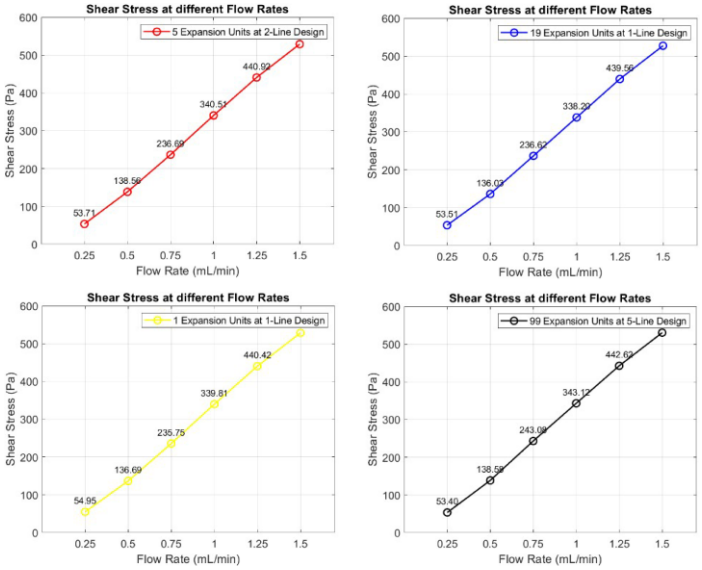

Fig.8: Shear stress at each design's first pair of teeth at different flow rates.

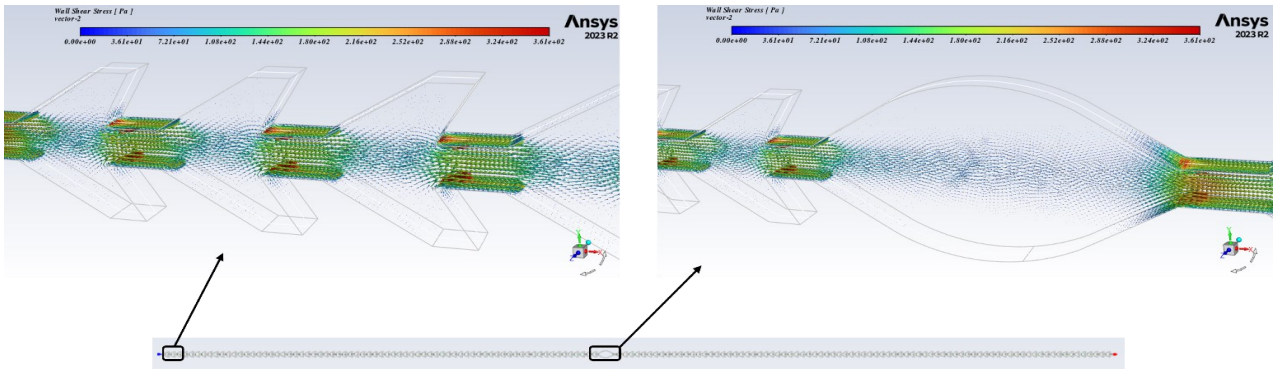

(a)

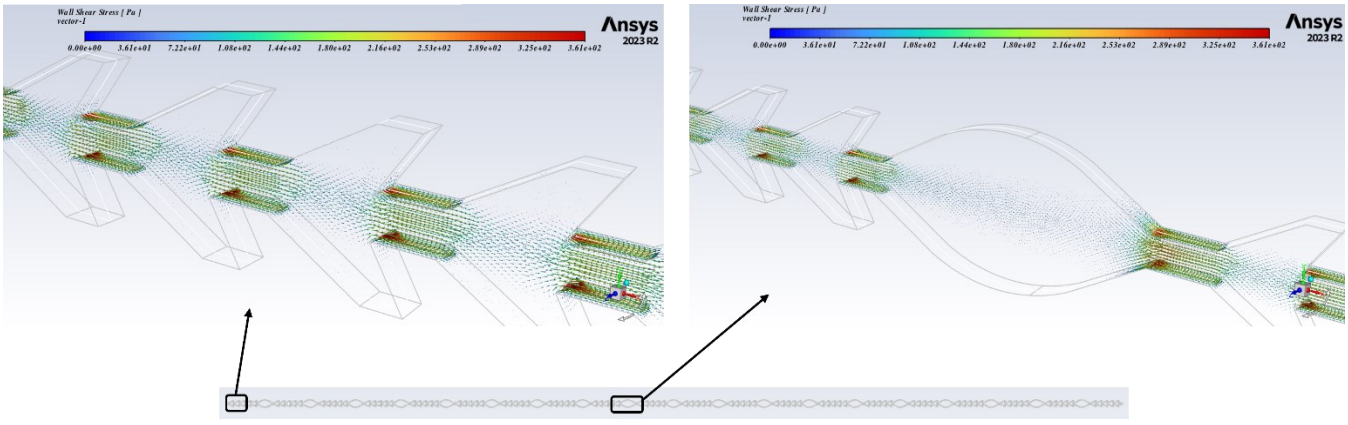

(b)

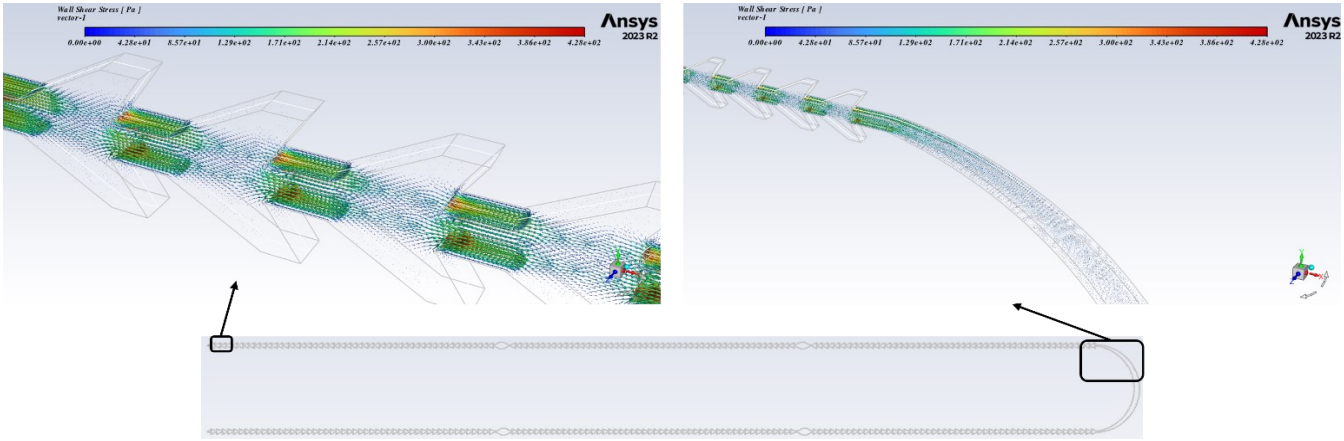

(c)

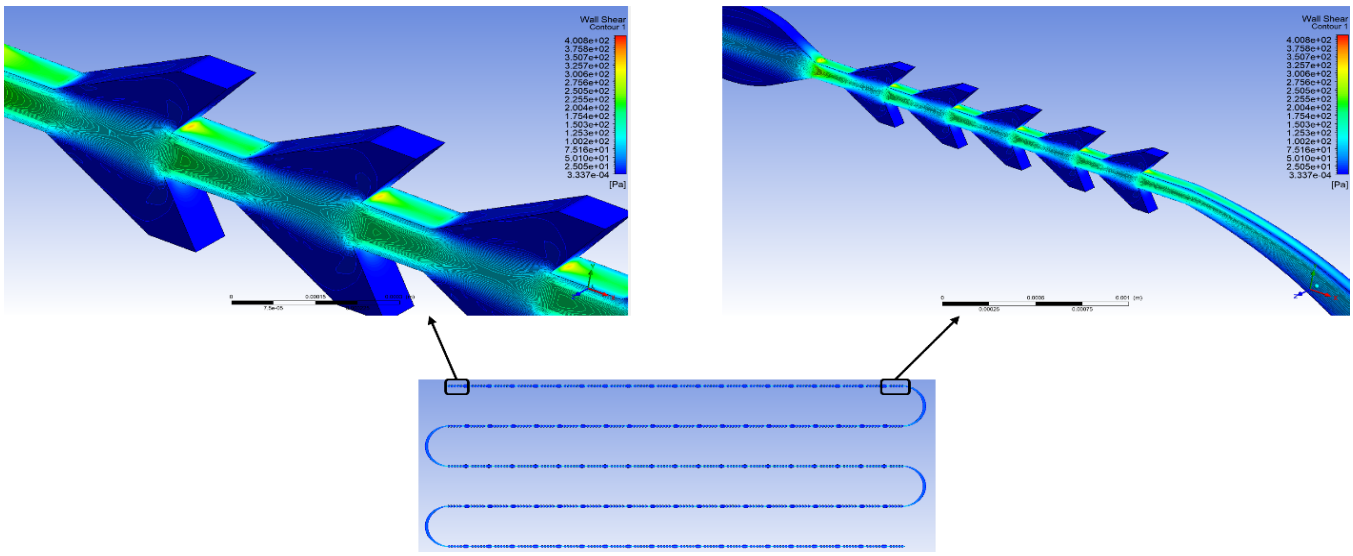

Fig.9: The simulation results of the chips on Ansys. (a) The first channel of chip A is "1 expansion unit at 1 line design". (b) The second channel of chip A is "19 expansion units at 1 line design". (c) Chip B is "5 expansion units at 2-line design". (d) Chip C is "99 expansion units at 5-line design".

Experimental Results

Following the analysis of simulation results, empirical laboratory experiments are performed to ascertain the appropriate design and effectiveness of modifying the expansion units in relation to denudation efficiency. Denudation efficiency refers to the ratio of denudated oocytes to the total number of (output) oocytes. Simulation results indicate that shear stress remains nearly uniform across all chip designs. Denudation efficiency will be calculated for each chip design. Figure 10 illustrates the denudation efficiency associated with each chip design. About 15 oocytes have been used at each group trial.

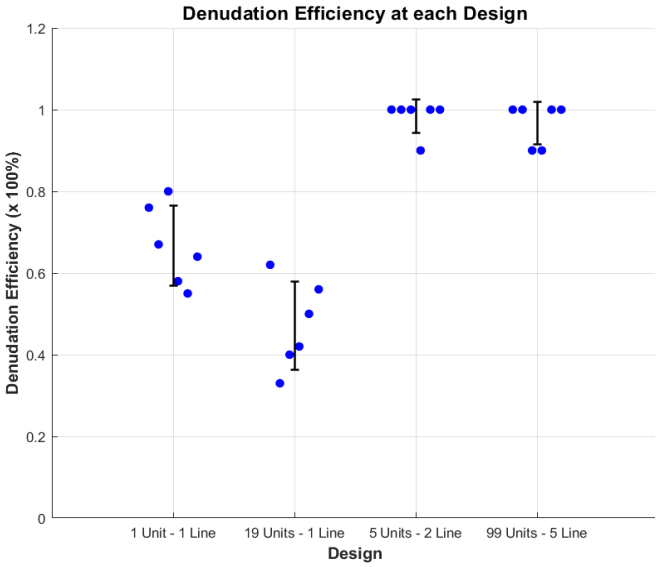

Fig.10: Denudation efficiency at the three chips. Where the first two channels belong to chip A, the third channel belongs to chip B, and the fourth channel belongs to chip C.

As seen in Figure 10, the highest denudation efficiency occurs at chip B and chip C. Chip B consists of 5 expansion units at a 2-line design and achieved almost 98.33% denudation efficiency. Chip C comprises 99 expansion units at a 5-line design, achieving almost 96.67% denudation efficiency. Efficiency decreased dramatically in chip A, reaching 66.67% at the first and 41.17% at the second channel. Error bars represent Standard Deviation (SD), which measures how much individual data points deviate from the mean of the dataset.

Discussion

By analyzing the results presented in Figures 8, 9, and 10, we can conclude that shear stress is crucial for denudation because it facilitates the mechanical removal of cumulus cells from the oocyte surface, reducing the need for enzymatic treatments. However, the number of jagged surfaces the oocytes encounter is a more influential factor, as it directly determines the extent of mechanical interaction and the effectiveness of cumulus cell detachment. To optimize the denudation process, oocytes must be exposed to an adequate number of jagged surfaces for efficient cumulus cell removal, while a sufficient number of expansion units is necessary to promote controlled oocyte rotation. This rotation ensures that all surfaces of the oocytes interact with the jagged structures, enhancing shear exposure and improving fluid dynamics within the microfluidic chip, ultimately leading to higher denudation efficiency.

When the flow rate decreases, the wall shear stress will be reduced, and the denudation efficiency will be reduced. If the flow rate increases, the output of oocytes will be reduced due to destruction. The optimal design that achieves the highest denudation efficiency without using enzymatic

action like hyaluronidase is the five expansion units at a 2-line design (one line measuring about 64.8 mm) at a constant flow rate of 1 mL/min. Figure 11 shows different shots of the complete denudated oocytes. Most oocytes show the polar body, indicating the perfect maturation and denudation process. Recent studies suggest that polar bodies play a role in embryonic development, and their form correlates with embryo quality and potential [70].

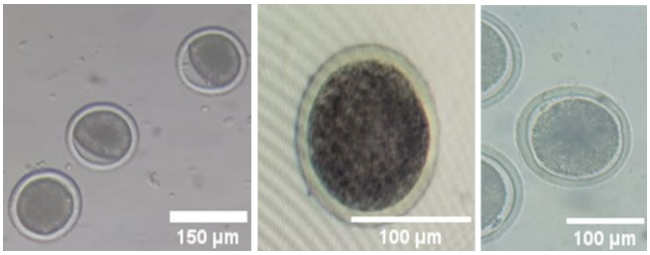

Fig.11: Shots of the complete denudated oocytes.

Figure 12 illustrates the incomplete denudated oocytes due to low wall shear stress or insufficient exposure to jagged surface units. As noted, cumulus corona cells remain around the oocytes, which can decrease the fertilization rate and harden the IVF of the ICSI process.

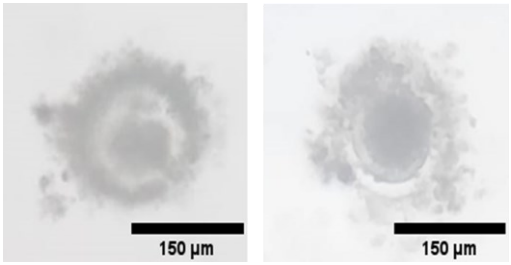

Fig.12: Shots of the incomplete denudated oocytes.

Figure 13 illustrates the mechanical interaction between the jagged surfaces, expansion units, and oocytes within the microfluidic channels. The input flow remains laminar, transporting un-denuded oocytes through the system. As the oocytes progress through the microfluidic chip, they encounter jagged surfaces, which generate localized shear stress to facilitate cumulus cell removal. Simultaneously, expansion units regulate the flow dynamics, promoting controlled oocyte rotation and ensuring uniform exposure to the shear forces. At the outlet, the oocytes emerge fully denuded, demonstrating the effectiveness of the microfluidic design in achieving efficient and consistent oocyte processing.

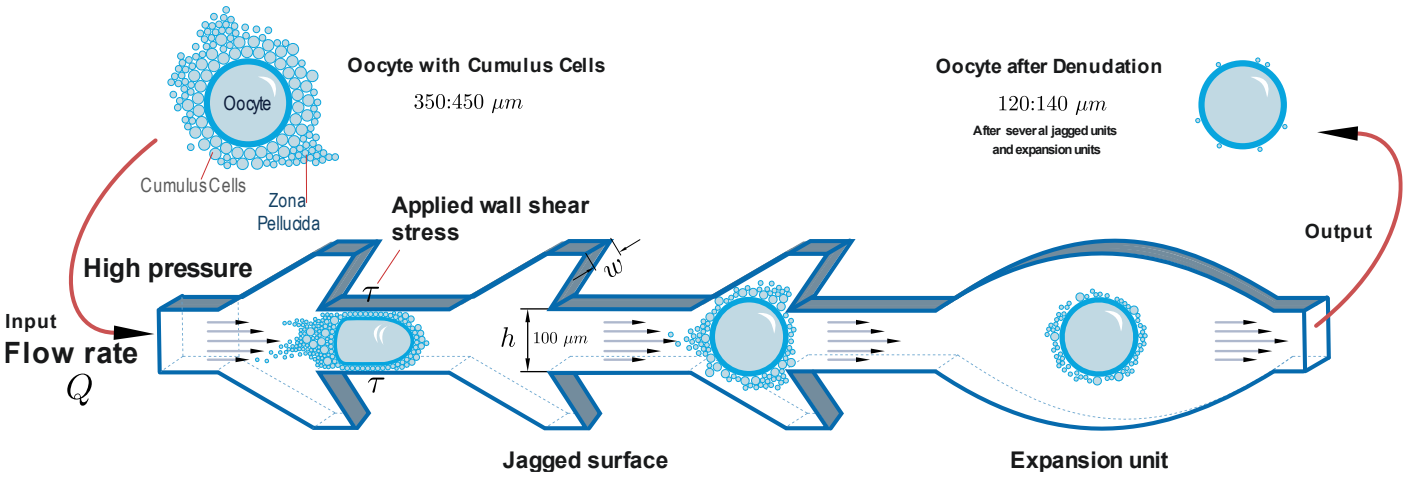

Fig.13: The mechanical concept of the microfluidic chips.

Conclusion

This study involved the design and manufacturing of microfluidic chips utilizing design software to test the effect of varying the number of expansion units in microfluidic chips for oocyte denudation, followed by the fabrication through direct CO_2 laser engraving on PMMA material to reduce the fabrication cost. The channels were divided into jagged surface units that remove the cumulus cells around the oocytes and expansion units to enhance fluid dynamics for soft cell processing. The configuration facilitates the transfer of oocytes through the chip, optimizes shear force to remove the cumulus-oocyte complexes without damaging the oocytes, and ensures that all surfaces of the oocytes are adequately exposed to the jagged surfaces. The PMMA material has demonstrated its suitability and efficiency in medical applications. Three chips with four designs have been designed and manufactured to test each design's shear stress and denudation efficiency. The chips consist of 3 layers; the middle layer thickness is 0.1 mm to ensure that the depth is constant through all chips. The chips' three layers were adjusted and thermally bonded in a natural ventilation lab oven at 150 degrees Celsius for 13 minutes under the force of 2 N. The fabrication duration was about 20 minutes, while the fabrication cost was about 1 USD. A Computational Fluid Dynamics (CFD) simulation was conducted using ANSYS Fluent 2023 R2. The process involved designing the model, applying mesh analysis with an element size of 10 µm, executing the setup and solution phases, and

rendering the results of wall shear stress. Almost the same level of wall shear stress was achieved at different chip designs while maintaining the tilting angle and flow rate. Therefore, real experimentation became essential to examine the impact of varying expansion units.

Different denudation efficiencies were obtained through the experimentation, and we found that chip B achieved 98.33% denudation efficiency, chip C achieved 96.67% denudation efficiency, the first channel in chip A achieved 66.67% denudation efficiency, and the second channel of chip A achieved 41.17%. The highest denudation efficiency at 98.33%, characterized by low cost and minimal fabrication time, was achieved with a design comprising five expansion units arranged in a 2-line design. This configuration is the best found among the existing ones because the oocytes are exposed to a reasonable number of continuous jagged surfaces and expansion units.

In the future work, it would be desirable to develop a develop a framework to automatically identify the efficiency of the oocyte output from the chips; as such the exploration of vision-based oocyte recognition and segmentation would facilitate the overall denudation process. We also plan to enable a low-cost actuation mechanism for an automated device in oocyte denudation schemes without using a syringe pump or related equipment to facilitate the denudation process.

Conflict of interest

Authors state no conflict of interest.

References

1. Hesam AA, Taghipour L, Rasekhi S, Fallahi S, Hesam Z. Investigating the Multiple Aspects of Mental Health in Infertile Women. Int J Ment Health Addict. 2017 Aug;15(4):928-32. https://doi.org/10.1007/s11469-016-9675-1
2. Ramírez-González JA, Vaamonde-Lemos R, Cunha-Filho JS, Varghese AC, Swanson RJ. Overview of the Female Reproductive System. In: Vaamonde D, Du Plessis SS, Agarwal A, editors. Exercise and Human Reproduction [Internet]. New York, NY: Springer New York; 2016 [cited 2024 Dec 16]. p. 19-46. https://doi.org/10.1007/978-1-4939-3402-7_2
3. Nicoloro-SantaBarbara JM, Lobel M, Bocca S, Stelling JR, Pastore LM. Psychological and emotional concomitants of infertility diagnosis in women with diminished ovarian reserve or anatomical cause of infertility. Fertil Steril. 2017 Jul;108(1):161-7. https://doi.org/10.1016/j.fertnstert.2017.05.008
4. Chen J, Fang Y, Xu Y, Sun H. Role of m6A modification in female infertility and reproductive system diseases. Int J Biol Sci. 2022;18(9):3592-604. https://doi.org/10.7150/ijbs.69771
5. Stejskalová A, Vankelecom H, Sourouni M, Ho MY, Götte M, Almquist BD. In vitro modelling of the physiological and diseased female reproductive system. Acta Biomater. 2021 Sep;132:288-312. https://doi.org/10.1016/j.actbio.2021.04.032
6. Zegers-Hochschild F, Adamson GD, Dyer S, Racowsky C, De Mouzon J, Sokol R, et al. The International Glossary on Infertility and Fertility Care, 2017. Fertil Steril. 2017 Sep;108(3):393-406. https://doi.org/10.1016/j.fertnstert.2017.06.005
7. Cox CM, Thoma ME, Tchangalova N, Mburu G, Bornstein MJ, Johnson CL, et al. Infertility prevalence and the methods of estimation from 1990 to 2021: a systematic review and meta-analysis. Hum Reprod Open. 2022 Sep 10;2022(4):hoac051. https://doi.org/10.1093/hropen/hoac051
8. Infertility Prevalence Estimates, 1990-2021. 1st ed. Geneva: World Health Organization; 2023. 1 p.
9. Katz P, Nachtigall R, Showstack J. The economic impact of the assisted reproductive technologies. Nat Cell Biol. 2002 Oct;4:S29-32. https://doi.org/10.1038/ncb-nm-fertilityS29
10. Chian RC, Lim JH, Tan SL. State of the art in in-vitro oocyte maturation: Curr Opin Obstet Gynecol. 2004 Jun;16(3):211-9. https://doi.org/10.1097/00001703-200406000-00003
11. Nosrati R, Graham PJ, Zhang B, Riordon J, Lagunov A, Hannam TG, et al. Microfluidics for sperm analysis and selection. Nat Rev Urol. 2017 Dec;14(12):707-30. https://doi.org/10.1038/nrurol.2017.175
12. Kashaninejad N, Shiddiky MJA, Nguyen N. Advances in Microfluidics‐Based Assisted Reproductive Technology: From Sperm Sorter to Reproductive System‐on‐a‐Chip. Adv Biosyst. 2018 Mar;2(3):1700197. https://doi.org/10.1002/adbi.201700197
13. Whitesides GM. The origins and the future of microfluidics. Nature. 2006 Jul;442(7101):368-73. https://doi.org/10.1038/nature05058
14. Sackmann EK, Fulton AL, Beebe DJ. The present and future role of microfluidics in biomedical research. Nature. 2014 Mar;507(7491):181-9. https://doi.org/10.1038/nature13118
15. Clark SG, Haubert K, Beebe DJ, Ferguson CE, Wheeler MB. Reduction of polyspermic penetration using biomimetic microfluidic technology during in vitro fertilization. Lab Chip. 2005;5(11):1229. https://doi.org/10.1039/b504397m
16. Suh RS, Zhu X, Phadke N, Ohl DA, Takayama S, Smith GD. IVF within microfluidic channels requires lower total numbers and lower concentrations of sperm. Hum Reprod. 2006 Feb 1;21(2):477-83. https://doi.org/10.1093/humrep/dei323
17. Han C, Zhang Q, Ma R, Xie L, Qiu T, Wang L, et al. Integration of single oocyte trapping, in vitro fertilization and embryo culture in a microwell-structured microfluidic device. Lab Chip. 2010;10(21):2848. https://doi.org/10.1039/c005296e
18. Wu J, Fang H, Zhang J, Yan S. Modular microfluidics for life sciences. J Nanobiotechnology. 2023 Mar 11;21(1):85. https://doi.org/10.1186/s12951-023-01846-x
19. Hassan HA. Clinical Assisted Reproduction: Cumulus Cell Contribution to Cytoplasmic Maturation and Oocyte Developmental Competence In Vitro. J Assist Reprod Genet. 2001 Oct 1;18(10):539-43.
20. De Vos A, Van Landuyt L, Van Ranst H, Vandermonde A, D'Haese V, Sterckx J, et al. Randomized sibling-oocyte study using recombinant human hyaluronidase versus bovine-derived Sigma hyaluronidase in ICSI patients. Hum Reprod. 2008 May 15;23(8):1815-9. https://doi.org/10.1093/humrep/den212

21. Rienzi L, Balaban B, Ebner T, Mandelbaum J. The oocyte. Hum Reprod. 2012 Aug 1;27(suppl_1):i2-21. https://doi.org/10.1093/humrep/des200
22. Chang MC. Fertilization of Rabbit Ova in vitro. Nature. 1959 Aug;184(4684):466-7. https://doi.org/10.1038/184466a0
23. Behringer R. Manipulating the mouse embryo: a laboratory manual. Fourth edition. Cold Spring Harbor, New York: Cold Spring Harbor Laboratory Press; 2014. 814 p.
24. Stern R, Jedrzejas MJ. Hyaluronidases: Their Genomics, Structures, and Mechanisms of Action. Chem Rev. 2006 Mar 1;106(3):818-39. https://doi.org/10.1021/cr050247k
25. Camaioni A, Hascall VC, Yanagishita M, Salustri A. Effects of exogenous hyaluronic acid and serum on matrix organization and stability in the mouse cumulus cell-oocyte complex. J Biol Chem. 1993 Sep;268(27):20473-81. https://doi.org/10.1016/S0021-9258(20)80750-9
26. Cross PC, Brinster RL. In Vitro Development of Mouse Oocytes1. Biol Reprod. 1970 Dec 1;3(3):298-307. https://doi.org/10.1093/biolreprod/3.3.298
27. Itagaki Y, Toyoda Y. Effects of Prolonged Sperm Preincubation and Elevated Calcium Concentration on Fertilization of Cumulus-Free Mouse Eggs in Vitro. J Reprod Dev. 1992;38(3):219-24. https://doi.org/10.1262/jrd.38.219
28. Evison M, Pretty C, Taylor E, Franklin C. Human recombinant hyaluronidase (Cumulase®) improves intracytoplasmic sperm injection survival and fertilization rates. Reprod Biomed Online. 2009 Jan;18(6):811-4. https://doi.org/10.1016/S1472-6483(10)60030-2
29. Taylor TH, Elliott T, Colturato LF, Straub RJ, Mitchell-Leef D, Nagy ZP. Comparison of bovine- and recombinant human-derived hyaluronidase with regard to fertilization rates and embryo morphology in a sibling oocyte model: a prospective, blinded, randomized study. Fertil Steril. 2006 May;85(5):1544-6. https://doi.org/10.1016/j.fertnstert.2005.10.053
30. Lee JH, Yoo M, Lee SM, Park SJ, Kil TY, Kim MK. Toxicity of the recombinant human hyaluronidase ALT-BC4 on embryonic development. J Anim Sci Technol. 2021 Mar;63(2):272-80. https://doi.org/10.5187/jast.2021.e34
31. Ishizuka Y, Takeo T, Nakao S, Yoshimoto H, Hirose Y, Sakai Y, et al. Prolonged exposure to hyaluronidase decreases the fertilization and development rates of fresh and cryopreserved mouse oocytes. J Reprod Dev. 2014;60(6):454-9. https://doi.org/10.1262/jrd.2014-045
32. Smith GD, Takayama S. Application of microfluidic technologies to human assisted reproduction. Mol Hum Reprod. 2017 Jan 27;gaw076. https://doi.org/10.1093/molehr/gaw076
33. Zeringue HC, Beebe DJ, Wheeler MB. Removal of Cumulus from Mammalian Zygotes using Microfluidic Techniques. Biomed Microdevices. 2001 Sep 1;3(3):219-24. https://doi.org/10.1023/A:1011463330597
34. Zeringue HC, Rutledge JJ, Beebe DJ. Early mammalian embryo development depends on cumulus removal technique. Lab Chip. 2005;5(1):86. https://doi.org/10.1039/b316494m
35. Weng L, Lee GY, Liu J, Kapur R, Toth TL, Toner M. On-chip oocyte denudation from cumulus-oocyte complexes for assisted reproductive therapy. Lab Chip. 2018;18(24):3892-902. https://doi.org/10.1039/C8LC01075G
36. Al-Halhouli A, Al-Faqheri W, Alhamarneh B, Hecht L, Dietzel A. Spiral Microchannels with Trapezoidal Cross Section Fabricated by Femtosecond Laser Ablation in Glass for the Inertial Separation of Microparticles. Micromachines. 2018 Apr 9;9(4):171. https://doi.org/10.3390/mi9040171
37. Chen Z, Memon K, Cao Y, Zhao G. A microfluidic approach for synchronous and nondestructive study of the permeability of multiple oocytes. Microsyst Nanoeng. 2020;6:55. https://doi.org/10.1038/s41378-020-0160-4
38. Mokhtare A, Davaji B, Xie P, Yaghoobi M, Rosenwaks Z, Lal A, et al. Non-contact ultrasound oocyte denudation. Lab Chip. 2022 Feb 15;22(4):777-92. https://doi.org/10.1039/D1LC00715G
39. Zhai R, Shan G, Dai C, Hao M, Zhu J, Ru C, et al. Automated Denudation of Oocytes. Micromachines. 2022 Aug 12;13(8):1301. https://doi.org/10.3390/mi13081301
40. Fang Y, Wu R, Lee JM, Chan LHM, Chan KYJ. Microfluidic in-vitro fertilization technologies: Transforming the future of human reproduction. TrAC Trends Anal Chem. 2023 Mar 1;160:116959. https://doi.org/10.1016/j.trac.2023.116959
41. Islam MdM, Loewen A, Allen PB. Simple, low-cost fabrication of acrylic based droplet microfluidics and its use to generate DNA-coated particles. Sci Rep. 2018 Jun 8;8(1):8763. https://doi.org/10.1038/s41598-018-27037-5
42. Nasser GA, Fath El-Bab AMR, Abdel-Mawgood AL, Mohamed H, Saleh AM. CO2 Laser Fabrication of PMMA Microfluidic Double T-Junction Device with Modified Inlet-Angle for Cost-Effective PCR Application. Micromachines. 2019 Oct 9;10(10):678. https://doi.org/10.3390/mi10100678
43. Adel M, Allam A, Sayour AE, Ragai HF, Umezu S, Fath El-Bab AMR. Fabrication of Spiral Low-Cost Microchannel with Trapezoidal Cross Section for Cell Separation Using a Grayscale Approach. Micromachines. 2023 Jun 30;14(7):1340. https://doi.org/10.3390/mi14071340
44. Mofadel H, Ali Hussein H, Fath El-Bab A, El-Sherry T. Bull sperm rheotaxis and kinematics in microfluidic channels with different heights. Assiut Vet Med J. 2023 Dec 23;0(0):0-0. https://doi.org/10.21608/avmj.2023.228274.1176
45. Mofadel HA, Hussein HA, Abd-Elhafee HH, El-Sherry TM. Impact of various cryo-preservation steps on sperm rheotaxis and sperm kinematics in bull. Sci Rep. 2024 May 18;14(1):11403. https://doi.org/10.1038/s41598-024-61617-y
46. Hashem R, El-Hussieny H, Umezu S, El-Bab AMRF. Soft Tissue Compliance Detection in Minimally Invasive Surgery: Dynamic Measurement with Piezoelectric Sensor Based on Vibration Absorber Concept. J Robot Control JRC. 2024 Jul 22;5(5):1399-411.
47. Prakash S, Kumar S. Fabrication of microchannels on transparent PMMA using CO2 Laser (10.6 µm) for microfluidic applications: An experimental investigation. Int J Precis Eng Manuf. 2015 Feb;16(2):361-6. https://doi.org/10.1007/s12541-015-0047-8
48. Helmy M, Fath El-Bab AM, El-Hofy H. Elimination of Clogging in PMMA Microchannels Using Water Assisted CO2 Laser Micromachining. Appl Mech Mater. 2015 Oct 19;799-800:407-12. https://doi.org/10.4028/www.scientific.net/AMM.799-800.407

49. Chen X, Li T, Shen J. CO2 Laser Ablation of Microchannel on PMMA Substrate for Effective Fabrication of Microfluidic Chips. Int Polym Process. 2016 May 29;31(2):233-8. https://doi.org/10.3139/217.3184
50. Imran M, Rahman RA, Ahmad M, Akhtar MN, Usman A, Sattar A. Fabrication of microchannels on PMMA using a low power CO2 laser. Laser Phys. 2016 Sep 1;26(9):096101. https://doi.org/10.1088/1054-660X/26/9/096101
51. Prakash S, Kumar S. Fabrication of rectangular cross-sectional microchannels on PMMA with a CO 2 laser and underwater fabricated copper mask. Opt Laser Technol. 2017 Sep;94:180-92. https://doi.org/10.1016/j.optlastec.2017.03.034
52. Mansour H, Soliman EA, El-Bab AMF, Abdel-Mawgood AL. Development of epoxy resin-based microfluidic devices using CO2 laser ablation for DNA amplification point-of-care (POC) applications. Int J Adv Manuf Technol. 2022 Jun;120(7-8):4355-72. https://doi.org/10.1007/s00170-022-08992-w
53. Nasser GA, Abdel-Mawgood AL, Abouelsoud AA, Mohamed H, Umezu S, El-Bab AMRF. New cost effective design of PCR heating cycler system using Peltier plate without the conventional heating block. J Mech Sci Technol. 2021 Jul;35(7):3259-68. https://doi.org/10.1007/s12206-021-0646-5
54. Ngum LF, Matsushita Y, El-Mashtoly SF, Fath El-Bab AMR, Abdel-Mawgood AL. Separation of microalgae from bacterial contaminants using spiral microchannel in the presence of a chemoattractant. Bioresour Bioprocess. 2024 Apr 13;11(1):36. https://doi.org/10.1186/s40643-024-00746-8
55. Wang L, Han J, Su W, Li A, Zhang W, Li H, et al. Gut-on-a-chip for exploring the transport mechanism of Hg(II). Microsyst Nanoeng. 2023 Jan 1;9(1):1-13. https://doi.org/10.1038/s41378-022-00447-2
56. Pan X, Chen J, Han J, Zhang W, Su W, Xu Z, et al. Critical Suitability Evaluation of Caco-2 Cells for Gut-on-a-Chip. ACS Appl Mater Interfaces. 2024 Sep 25;16(38):51139-49. https://doi.org/10.1021/acsami.4c11409
57. Kyogoku H, Kitajima TS. The large cytoplasmic volume of oocyte. J Reprod Dev. 2023;69(1):1-9. https://doi.org/10.1262/jrd.2022-101
58. Raghu HM, Nandi S, Reddy SM. Follicle size and oocyte diameter in relation to developmental competence of buffalo oocytes in vitro. Reprod Fertil Dev. 2002;14(1):55. https://doi.org/10.1071/RD01060
59. Turathum B, Gao EM, Chian RC. The Function of Cumulus Cells in Oocyte Growth and Maturation and in Subsequent Ovulation and Fertilization. Cells. 2021 Sep 2;10(9):2292. https://doi.org/10.3390/cells10092292
60. Del Bianco D, Gentile R, Sallicandro L, Biagini A, Quellari PT, Gliozheni E, et al. Electro-Metabolic Coupling of Cumulus-Oocyte Complex. Int J Mol Sci. 2024 May 14;25(10):5349. https://doi.org/10.3390/ijms25105349
61. Govahi A, Eghbali S, Ghiasi NE, Zandieh Z, Ajdary M, Mehdizadeh R, et al. Changes in the transcriptomic profile of cumulus cells under the influence of cumulus-oocytes complex pre-incubation. Sci Rep. 2024 Jul 26;14(1):17183. https://doi.org/10.1038/s41598-024-66822-3
62. Quispe-Gutiérrez US, Olivera-Marocho LV, Ccopa Ccallata J, Pahuara Farfan LE, Barragán-Condori M, Berndtson JL. Effect of FSH and eCG on alpaca (Vicugna pacos) oocyte maturation in vitro. 2021 Jul 15 [cited 2024 Dec 17]; Available from: https://hdl.handle.net/20.500.12955/2133
63. Pelesko JA, Bernstein DH. Modeling MEMS and NEMS [Internet]. 0 ed. CRC Press; 2002 [cited 2024 Dec 16]. https://doi.org/10.1201/9781420035292
64. Tao R, Ng T, Su Y, Li Z. A microfluidic rectifier for Newtonian fluids using asymmetric converging-diverging microchannels. Phys Fluids. 2020 May 1;32(5):052010. https://doi.org/10.1063/5.0007200
65. Panigrahi PK. Transport Phenomena in Microfluidic Systems [Internet]. 1st ed. Wiley; 2016 [cited 2024 Dec 16]. https://doi.org/10.1002/9781118298428
66. Kim TH, Lee JM, Ahrberg CD, Chung BG. Development of the Microfluidic Device to Regulate Shear Stress Gradients. BioChip J. 2018 Dec;12(4):294-303. https://doi.org/10.1007/s13206-018-2407-9
67. Bruus H. Acoustofluidics 1: Governing equations in microfluidics. Lab Chip. 2011;11(22):3742. https://doi.org/10.1039/c1lc20658c
68. Rossi M, Lindken R, Hierck BP, Westerweel J. Tapered microfluidic chip for the study of biochemical and mechanical response at subcellular level of endothelial cells to shear flow. Lab Chip. 2009;9(10):1403. https://doi.org/10.1039/b822270n
69. Aung HH, Pothipan P, Aswakool J, Santironnarong S, Phatthanakun R, Pinrod V, et al. Non-invasive measurement of wall shear stress in microfluidic chip for osteoblast cell culture using improved depth estimation of defocus particle tracking method. Biomicrofluidics. 2024 Sep 1;18(5):054114. https://doi.org/10.1063/5.0226294
70. Yang Y, Tan W, Chen C, Jin L, Huang B. Correlation of the position and status of the polar body from the fertilized oocyte to the euploid status of blastocysts. Front Genet. 2022 Sep 20;13:1006870. https://doi.org/10.3389/fgene.2022.1006870